Journal of Materials Chemistry A

Accepted Manuscript

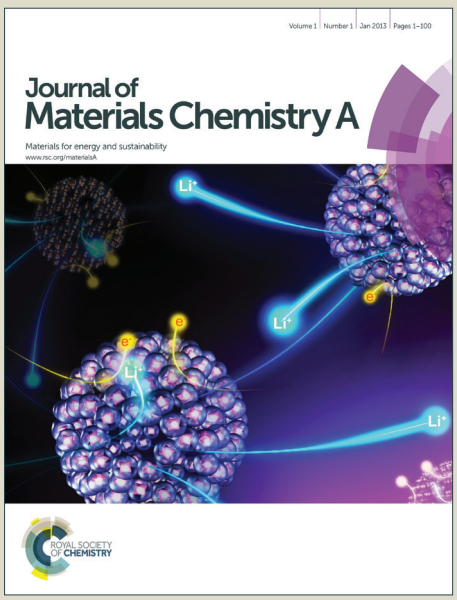

ROYAL SOCIETY OF CHEMISTRY

www.rsc.org/materialsA

Journal of Material Chemistry A

RSCPublishing

ARTICLE

Facile Potentiostatic Preparation of Functionalized Polyterthiophene Anchored Graphene Oxide as Metal-Free Electrocatalyst for Oxygen Reduction Reaction

Cite this: DOI: 10.1039/x0xx00000x

Received 00th January 2012,
Accepted 00th January 2012

DOI: 10.1039/x0xx00000x

www.rsc.org/

M. Halappa Naveen,[a] Hui-Bog Noh,[a] Md Shahriar Al Hossain,[b] Jung Ho Kim,*[,b] and Yoon-Bo Shim*[,a]

Finding a new catalyst for high-performance, cost-effective oxygen reduction is crucial for the commercialization of fuel cells. Herein, we have demonstrated functionalized polyterthiophenes anchored graphene oxide (GO) as new non-metal catalysts for the oxygen reduction reaction (ORR). Different functional groups containing monomers, 3′-(2-aminopyrimidyl)-2,2′:5′,2″-terthiophene (APT), 3′-(p-benzoic acid)-2,2′:5′,2″-terthiophene (TBA), and 3′-(carboxylic acid)-2,2′:5′,2″-terthiophene (TCA), were synthesized and polymerized with the as-prepared GO and monomer complexes by the potential cycling method. Of these, aminopyrimidyl groups on poly(APT) backbone serves effective functionalities for the ORR. The APT-GO complex was formed through hydrogen bonding and ring opening reaction of epoxide group with amine to form a new C–N bond. It was observed that C–N bond in the polymer matrix mainly involved in the electrocatalytic reduction of O_2 to H_2O directly. The poly(APT-GO) revealed much better tolerance to the fuel crossover and long term electrode stability than that of commercially available Pt-C.

Introduction

Catalytic oxygen reduction is a crucial research topic due to its fundamental role in fuel cells (FCs).[1-4] The development of a practical electrocatalyst for the oxygen reduction reaction (ORR) still has not overcome its sluggish kinetics. In recent years, the most effective electrocatalyst for the ORR has been found to be precious metals such as platinum (Pt) and its alloys,[5, 6] which possess superb catalytic properties for commercial FCs. The exclusive dependence on expensive Pt for FCs, however, has been unavoidable as a major obstacles to commercialize this attractive energy conversion technique. Thus, greater efforts have been expended to replace this expensive metal with highly active, durable, and inexpensive non-metals such as carbon or metal composite catalysts.[2,7-9] To fulfil these requirements, the electrically conductive π-conjugated polymers (ECPs) are being considering as acceptable candidates in terms of cost-effectiveness and high-performance.

Since the discovery of ECPs, they have become attractive because of their fascinating electronic and physical properties, such as tunable band gaps, redox properties, resistance against corrosion, and low materials cost. Moreover, the ECPs have received significant attention due to their various applications such as sensors, batteries, electronic devices, etc.[10-14] Interestingly, heteroatom-substituted ECPs have provided polymer-based photocatalysts with enhanced activity for hydrogen production.[15] Limited works has been reported to date, however, on using ECPs for the ORR, and the existing reports have mostly used composites of heterocyclic ECPs with metal ions.[16-20] Using non-metal composites with ECPs is still challenging because they always show insufficient performance for the ORR.[4,21-24] To explore the possibility of using non-metals, graphene oxide (GO) and doped graphene composites can be suggested as a potential candidate because of its abundant oxygen groups that promote functionalization for potential active and conductive sites.[25]

GO has been a strong candidate in a wide range of application fields, such as electronics, sensors, batteries, solar cells, and catalysts, due to its excellent physical and chemical properties.[26-28] The facile chemical functionalization of GO provides a much more effective way to endow graphene with new features and resolve its re-aggregation problem, which greatly hinders its applications. More interestingly, the

properties of π-conjugated polymer anchored GO are expected to improve ion conductivity, mechanical strength, and thermal stability. It is therefore hypothesized that the incorporation of GO into the ECP matrix could improve its conductivity and reduce the biofouling of the matrix for catalytic applications.[29] In addition, sulfur atom in the polymer backbone serves as active sites for ORR.[30] Such a composite represents a new non-metal catalyst for the ORR that exhibits stable activity through the effective interaction between amine and carboxylic groups attached to organic conjugated polymers and the oxygen-containing groups of GO, allowing the formation of a uniform homogeneous electrode surface.

In the present study, we describe the preparation of this new electrocatalyst for the ORR, in which the catalysts were prepared electrochemically from monomers, containing different functional groups (3′-(2-aminopyrimidyl)-2,2′:5′,2″-terthiophene) (APT), (3′-(carboxylic acid)-2,2′:5′,2″-terthiophene) (TCA), and 3′-(*p*-benzoic acid)-2,2′:5′,2″-terthiophene (TBA), and GO in complexes. The resulting complexes and catalyst materials were characterized by Fourier transform infrared spectroscopy (FTIR), thermogravimetric analysies (TGA), field emission-scanning electron microscopy (FE-SEM), high resolution transmission electron microscopy (HR-TEM), X-ray photoelectron spectroscopy (XPS), electrochemical impedance spectroscopy (EIS), and voltammetry. Furthermore, the electrochemical behavior and electron transfer number (*n*) of these composites involved in the ORR were evaluated by rotating disk electrode (RDE) experiments under fuel cell operating conditions. The kinetic and electrocatalytic activities of these materials towards the ORR were also calculated from the well-known Koutecky-Levich equation and Tafel plots.

Experimental

Synthesis of Material

GO was prepared from natural graphite flakes using a previously reported improved Hummer's method.[28] Graphite powder and all chemicals were purchased from Sigma Aldrich (USA) and used without further purification. Acetonitrile (≥99.8%, anhydrous, sealed under N_2 gas) was purchased from Sigma–Aldrich Co. Tetrabutylammonium perchlorate (TBAP, electrochemical grade) was obtained from the Fluka Co. (USA) and dried under vacuum (10^{-5} Torr). Chromatographic purification of products was carried out using silica gel, 70-230 mesh. All aqueous solutions were prepared in double-distilled water, which was obtained from a Milli-Q water purifying system (18 MΩ cm). The freshly prepared GO was dispersed in an acetonitrile solution by ultrasonication for one hour to obtain a homogeneous stable GO dispersion. The monomer precursors of the conducting polymers (APT, TCA, and TBA) were synthesized by a procedure reported previously in our group.[13,31,32] The terthiophene starting molecule, benzotrithiophene (BTT) was prepared from 2,3,5-tribromothiophene by a one-step procedure. Then, the BTT was converted to terthiophene boronic (TTB) acid in the presence of *n*-BuLi and trimethyl borate. The final monomer product was synthesized by the Suzuki coupling reaction between TTB and 2-amino-5-bromopyrimidine to form APT. Recrystallization from ethanol provided 2.05 g of greenishyellow solid. MP: 192.7-194.1 °C. IR (KBr): 3315 cm^{-1}, 3165 cm^{-1}, 1663 cm^{-1}, 1495 cm^{-1}; ^{1}H-NMR ($CDCl_3$) δ: 5.34 (s, 2H), 6.96–6.99 (m, 1H), 7.02–7.08 (m, 3H), 7.20–7.24 (m, 3H), 8.34 (s, 2H); ^{13}C-NMR ($CDCl_3$) δ: 120.2, 124.2, 125.0, 125.9, 126.4, 126.9, 127.5, 128.0, 131.1, 133.0, 134.8, 136.3, 136.4, 158.2, 162.1; HRESI-MS $[M+H]^+$: m/z calcd for 341.0115, found 341.0110. TCA was synthesized from BTT by a two-step process. Terthiophene bromide was refluxed with cuprous cyanide in dimethylformamide (DMF) to give 3′-cyano-5,2′-5′2-terthiophene (CTT). The resulting CTT was hydrolyzed by KOH to give the desired TCA. Recrystallization from ethanol provided 2.69 g (92%) of yellow needles. MP: 192.7-194.1 °C. IR (KBr) 1677 cm^{-1}, 2500-3100 (br) cm^{-1}; ^{1}H-NMR ($CDCl_3$) δ: 7.04-7.59 (m, 6H), 7.59 (s, 1H); ^{13}C-NMR ($CDCl_3$) δ; 125.0, 125.9, 126.9, 127.8, 128.4, 128.6, 130.2, 133.6, 135.9, 136.1, 143.8, 166.7; HRESI-MS $[M+H]^+$: m/z calcd for 292.3894, found 292.3802. TBA was obtained by a two-step procedure in which the first step is a simple Suzuki coupling between TTB and 4-bromobenzonitrile to form 3'-(4-benzonitrile)-2, 2′:5′, 2″-terthiophene (BNTT), and the second step is the hydrolysis of BNTT in the presence of KOH and a mixture of ethoxyethanol/water. Recrystallization from ethanol provided 2.93 g (80%) of yellow needles. MP: 127–128.3 °C. IR (KBr) 250–3400 cm^{-1} (br, OH), 1660 cm^{-1} (C=O), 1510 cm^{-1}, 1417 cm^{-1} (C–S, thiophene); ^{1}H-NMR ($CDCl_3$) δ: 6.22 (s, 1H), 6.91–7.08 (m, 4H), 7.17 -7.28 (m, 3H), 7.50 (d, 2H), 7.83 (d, 1H); ^{13}C-NMR ($CDCl_3$) δ: 124.7, 124.7, 126.1, 126.8, 127.2, 127.4, 127.7, 128.5, 128.8, 129.8, 133.4, 34.1, 135.2, 135.4, 137.9, 138.6, 167.4; HRESI-MS $[M+H]^+$: m/z calcd for 368.0042, found 368.0031. The synthesized monomers were added to the GO suspension, which was further sonicated for 1 h to obtain a homogeneous mixture of monomer-GO suspension. An optimized ratio of monomer to GO (1:1) was used to obtain a homogeneous solution without significant agglomeration of GO with the monomer. The electrochemical polymerization was achieved in an acetonitrile solution containing the mixture of APT monomer and GO with 0.1 M TBAP by scanning the potential three times from 0.0 to 1500 mV at a scan rate of 100 mV/s. After polymerization, the GO-containing poly(APT-GO) was washed with acetonitrile to remove any freely bonded monomer and GO. The identical experimental conditions were used for the preparation of poly(TCA-GO) and poly(TBA-GO). For comparison, pure polymer film electrodes were prepared by using only monomer without GO under identical experimental conditions, and reduced graphene oxide (RGO)-containing polymer (poly(APT-RGO)) was also prepared for comparison with poly(APT-GO).

Instruments

^{1}H and ^{13}C nuclear magnetic resonance (NMR) spectra were collected using a Bruker Advance 300 Spectrometer, with $CDCl_3$ as a solvent. Tetramethylsilane (TMS) was used as an internal standard. The FTIR spectra were collected using a JASCO FTIR spectrometer. The prepared polymer-GO material was characterized using multiple physicochemical techniques. The morphology of the material surface was confirmed by FE-SEM and HR-TEM images (TEM: LIBRA 200Cs (Carl Zeiss)). XPS on a Multilab 2000 (Thermo Fisher Scientific, UK) with an Al K^+ source at the Korea Basic Science Institute (KBSI, Busan) was used to analyze the elements present on the polymer-GO film electrode. Electrochemical measurements were conducted using a Kosentech bipotentiostat (Model Bipot-1, S. Korea) in a conventional three-electrodes assembly with glassy carbon (GC) and polymer layers (area: 0.196 cm^2) as working electrodes, platinum wire as the auxiliary electrode, and silver/silver chloride (Ag/AgCl sat'd. KCl) as a reference electrode. (All experiments were performed using the same reference electrode.) EG&G Princeton Applied Research PARSTAT 2263 was used to collect the impedance spectra at open circuit voltage from 100.0 kHz to 100.0 mHz (AC amplitude: 10.0 mV). RDE measurements were performed using the RDE system of EG&G PARC Model 636. For the control experiments, a carbon-supported Pt electrode was prepared by drop casting on the GC surface, using a dispersed slurry of commercially available 60% Pt/C (1 mg/ml) in an acetonitrile solution.

Results and discussion

Formation of monomer-GO complex

Scheme 1. Schematic representation of the preparation method for the polymer-GO composite electrode for ORR.

Three different monomers, APT, TBA, and TCA, were proposed and obtained as monomer-GO complexes through hydrogen bond formation. Among these, only APT-GO monomer allows self-assembly into a homogeneous complex without any aggregation between the GO nanosheets. The detailed procedure is shown in Scheme 1. The mixed solution of GO and the APT monomer allows the opening of the epoxy ring and their interaction with each other. It has been reported that one-step epoxy ring opening reaction occurs between the amino groups of the monomer and the epoxy groups of GO.[33] Herein, electrostatic interaction between the $–COO^-$ and the protonated $–NH_2^+$ groups allowe the formation of a homogeneous APT-GO suspension in the aprotic solvent. We expected that the formation of the homogeneous APT-GO suspension would result in the formation of a uniform poly(APT-GO) layer on the electrode surface by the potential cycling method. This can be further confirmed by FTIR spectra of the monomers and the complex (GO, APT, and APT-GO), which elucidate the interaction between the APT and the GO. As shown in Figure 1(a), the characteristic absorption bands of unmodified GO appear at 3417 (O–H stretching), 1690 (C=O (carbonyl) stretching vibration), 1222 (C–O stretching in the epoxy group), and 1083 cm^{-1} (C–O bond stretching in the alkoxy group), which are in good agreement with the frequency values reported in the literature.[34] Obviously, the spectrum of the APT monomer shows N–H stretching vibration bands of the primary amine at 3157 and 3318 cm^{-1}, and the N–H bending of the NH_2 group is observed at 1663 cm^{-1}. In addition, the stretching band of the C–N bond appears at 1605 cm^{-1}. That is to say, these observations are within the limit of detection. After the reaction between the APT monomer and the GO, the relative intensities of the corresponding bands of the active groups change significantly. The GO has been reported to contain reactive epoxy groups,[35] leading to a reaction with the amine groups via a well-known ring opening reaction of the active epoxide ring and the amine group to form a new C–N bond. As evidence for the above statement, the magnified spectra replotted in Figure 1(b) demonstrate that the relative intensity of the epoxy C–O stretching vibrations (1265 cm^{-1}) is significantly decreased in the APT-GO sample. Moreover, the increased intensity of the C–N stretching band at 1549 cm^{-1} suggests the formation of the new bond. The decreased intensity and broadened carboxyl C–O stretching band also shifts to 1744 cm^{-1}. These results can be attributed to the existence of an interaction between carboxylic acids and the amine groups. To further confirm these, TCA and TBA monomer complexed GO were further investigated to gain deeper insight into the functionalization of these two monomers. As shown in Figure 1(c), the C–O stretching vibration reflected by the epoxy and carbonyl stretching bands remains in the same position in both the TCA-GO and the TBA-GO composites. The functional group bands in the composite spectra of both samples remain in the same positions with the same intensity, indicating a weak interaction between the GO and the carboxylic-group-bearing monomers.

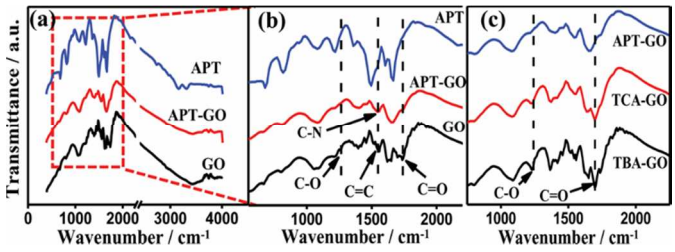

Figure 1. FTIR spectra of GO, APT, and APT-GO composite: (a) full scale spectra, (b) magnified spectra, and (c) comparison of FTIR spectra for APT-GO, TCA-GO, and TBA-GO.

The thermal properties of GO, APT, TBA-GO, TCA-GO and APT-GO were examined under N_2 flow, heated up to 800 °C at a rate of 10 °C·m^{-1}, as shown in Figure 2(a). The different monomer-GO composite suspensions were dried completely at room temperature to obtain solid-state specimens. The thermal analysis of all the samples revealed that GO starts to dramatically lose weight at around 152 °C because of the thermally unstable oxygen functional groups present on its surface. The APT monomer, which loses weight from 288 °C, shows better thermal stability. Otherwise, thermal degradation (T_d) of the APT-GO takes place at 185 °C with 20% weight loss, while GO and APT degrade at 124 and 257 °C with over 80% weight loss. Very interestingly, the APT-GO exhibits the most improved thermal stability compared to that of any other GO complexs. In details, APT-GO loses only 40% of its weight, even at 800 °C, whereas both the APT and the GO lose 80% of their initial weight. This is mainly because the APT monomer consists of a thermally stable terthiophene backbone, resulting in excellent thermal properties.[36] For a comparative study, the thermal stability of the TCA-GO and TBA-GO complexes was also investigated. Even though they exhibited better thermal properties than pure GO, they showed severe weight loss: A 45% weight loss was observed for TBA-GO and a 57% weight loss for TCA-GO. This better stability can be attributed to the formation of hydrogen bonds between the TCA and TBA monomers and the GO. In addition, TCA and TBA contain carboxylic groups, and these groups may undergo hydrogen bond formation with GO functional groups. The formation of hydrogen bonds explains the good stability of the two samples. In addition, polymer composites exhibits higher T_d value than that of monomer-GO complexes. The T_d for poly(APT-GO) is 315 °C, whereas poly(TBA-GO) and poly(TCA-GO) exhibit 298 and 295 °C respectivelly. This results suggest that poly(APT-GO) electrode exihibited highest thermal properties than that of corresponding polymer composites and precursor materials. When different content ratios of APT to GO were loaded, as shown in Figure 2(b), a slight improvement in stability was observed with increasing amounts of APT, and all compositions were more thermally stable at higher content ratio. This indicates that an increasing amount of APT increases thermal stability for the GO-APT complex.

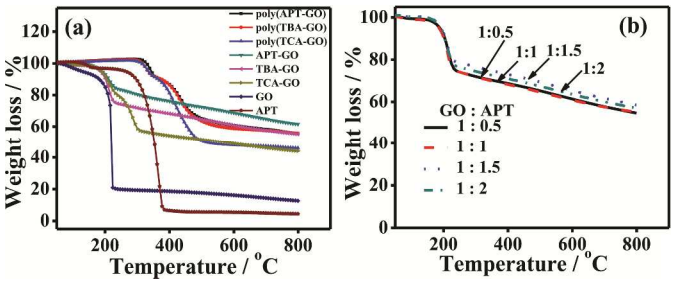

Figure 2. TGA curves of (a) poly(APT-GO), poly(TBA-GO), poly(TCA-GO), GO, APT, APT-GO, TCA-GO, and TBA-GO, and (b) different weight ratios of APT-GO composite.

The morphologies of GO, APT-GO, and the electrochemically polymerized APT-GO (hereafter, poly(APT-GO)) complex are shown in Figure 3. The GO-anchored polymer electrode was prepared by the potential cycling method with the monomer-GO complex in an acetonitrile solution. Figure 3(a) and (b) shows FE-SEM images of the as-prepared GO (consisting of a single layer of nanosheets) and of APT-GO. It should be noted that there is no noticeable difference between the two samples, although the poly(APT-GO) image shown in Figure 3(c) obviously reveals that the GO layer includes rough and aggregated polymer networks. In this case, the network structure of the poly(APT-GO) leads to highly dense and conductive properties. This morphology also provides a large surface area and helps to form more active sites on the electrode surface to attract oxygen molecules, which would be an important factor that would help the ORR to achieve superior electrochemical performance. Figure 3(d-f), shows the graphical patterns of the corresponding specimens. Detailed HR-TEM observations of the GO show the typical single layer transparent flake shape of a GO sheet (Figure S1(a) in the Supporting Information (SI)), where the inset in Figure S1(b) (SI) is the fast Fourier transform (FFT) pattern of a single layer GO sheet. It is worth noting that the polycrystalline nature of the surface on the polymer-GO composite material (Figure 3(g)) is confirmed, showing the presence of GO lattice fringes and GO surrounded by polymer (inset of Figure 3(g)). Since the polymer is anchored with GO through electropolymerization, it is reasonable to find the GO fringes in the polymer layer.

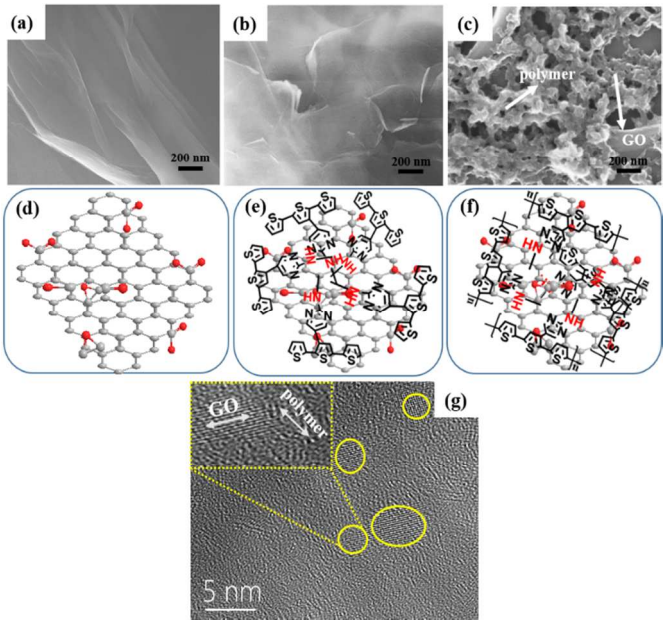

Figure 3. FE−SEM images of (a) GO, (b) APT-GO, and (c) poly(APT-GO). (d), (e), and (f) are the schematic patterns of the corresponding images. (g) HR-TEM image of the poly(APT-GO) layer. The yellow ellipses indicate GO surrounded by polymer.

The formation of complexes of APT, TCA, and TBA monomers with GO, such as APT-GO, TCA-GO, and TBA-GO, can be further supported by XPS. Spectra of all the samples are presented in Figure S2(a) in the SI. As shown in Figure S2(b) (SI), the high resolution C 1s spectrum of the APT-GO sample reveals the binding energies at 284.5 (C–C), 285.6 (C–OH), and 288.3 eV (C=O). In addition, a new peak at 286.9 eV(C–N) was observed indicating the interaction of the amine group with GO.

Neither TCA-GO (Figure S2(c) in the SI) nor TBA-GO (Figure S2(d) in the SI), however, exhibited any evidence of C–N.

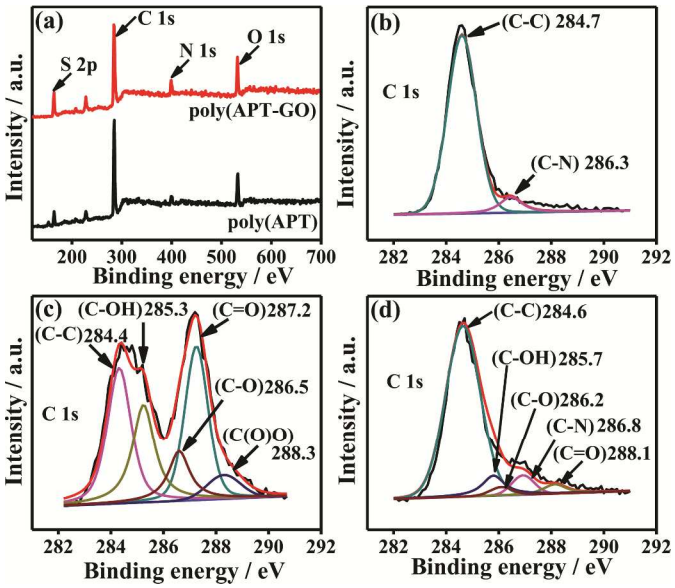

Figure 4. (a) XPS survey spectra of poly(APT-GO) and poly(APT) samples; high resolution C 1s spectra of (b) poly(APT), (c) GO, and (d) poly(APT-GO).

After the polymerization, a detailed XPS analysis was further conducted. Figure 4(a) shows the survey spectra of the poly(APT-GO) and poly(APT) samples. As can be seen here, there is no noticeable change. The C 1s binding energies of the poly(APT) were observed at 287.4 and 286.3 eV, corresponding to C–C and C–N bonds (Figure 4(b)). To further clarify the role of the as-prepared GO, the C 1s spectrum is shown in Figure 4(c) separately. It was observed that there were functional groups at 284.4 (C–C), 285.3 (C–OH), 286.5 (C–O), 287.2 (C=O), and 288.3 eV (O–C=O), respectively.[37] Surprisingly, the high resolution C 1s XPS spectrum of poly(APT-GO) shown in Figure 4(d) reveals a significantly decreased carbon component (C-O) on the epoxy group at 286.2 eV, where shifting of the binding energy is observed. The binding energies corresponding to the C 1s component of graphene oxide are observed, while they are not observed in the C 1s spectrum of the poly(APT) sample. A new peak with increased intensity is observed at 286.8 eV, however, which indicates C–N bond formation between the APT and the GO. The N 1s core level spectra for poly(APT) and poly(APT-GO) are shown in Figure S3(a-(i) and a-(ii)) in the SI. It confirms the aminopyrimidine group presenting on the electrode surface. The spectrum for the poly(APT) layer shows three differentiated peaks at 398.9 eV for C=N–, at 400.0 eV for –NH–, and at 401.1 eV, corresponding to protonated primary amine nitrogen, $–NH_2^+–$. The small shift of the C=N– peak to a higher binding energy value suggests the functionalization of the amine groups. In detail, the shifting of the binding energy of the NH_2 group to a higher binding energy (from 401.1 to 401.7 eV) is due to hydrogen bonding involving the amine group and the GO functional groups. In Figure S3(b) (SI), the peaks are observed at 163.5 and 164.4 eV, and both are attributed to the sulfur species from poly(APT-GO). This experimental result confirms interaction between the APT and the GO functional groups in the polymer. The quantity of the elements determined by XPS data, it suggest that the 72.3 % of carbon, 11.3 % of oxygen, 8.48 % of Nitrogen, and 7.85 % of sulfur.

Electrochemical impedance spectroscopy (EIS) was necessary to evaluate the charge transport properties of the electrode material. This was performed in 0.1 M KCl containing 4.0 mM $Fe[(CN)_6]^{3-/4-}$/0.3 M $NaClO_4$. The EIS spectra for poly(APT), GO, and poly(APT-GO) are shown in Figure 5. The collected data were quantitiatively analyzed using an equivalent circuit (inset of Figure 5), in which R_s represents the solution resistance, Q represents the constant phase element, R_{ct} represents the charge transfer resistance, R_f represents the film resistance, and W represents the Warburg element. All the Nyquist plots show a semicircular arc within the frequency range from 100 kHz to 100 mHz at open circuit potential, which is related to the interfacial charge transfer process. The R_{ct} values were 1.52, 0.43, and 0.88 kΩ for the GO, the poly(APT), and the poly(APT-GO)), respectively. Poly(APT) contains NH_3^+ groups on its surface, which facilitates the interfacial charge transfer process in the $Fe[(CN)_6]^{3-/4-}$/0.3 M $NaClO_4$ containing solution.

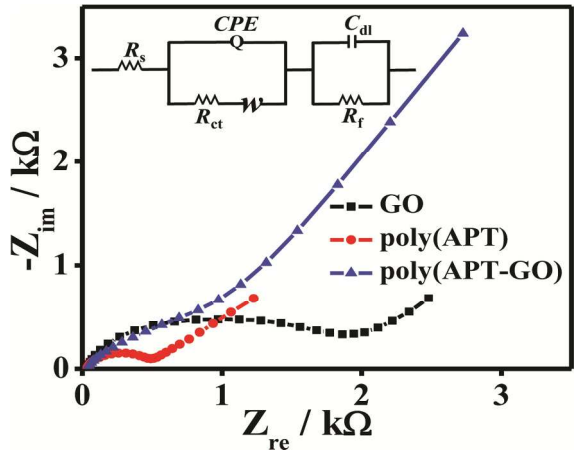

Figure 5. Nyquist plots obtained for GC/GO, GC/polyAPT, and GC/poly(APT-GO) electrodes in 0.1 M KCl containing 4.0 mM $Fe[(CN)_6]^{3-/4-}$/0.3 M $NaClO_4$. (Inset shows the equivalent circuit for the corresponding data.)

The GO surface has a higher R_{ct} (larger semicircle) because the negative charge on the GO surface repulses the negatively

charged ferrocyanide/ferricyanide redox couple. The interfacial resistance of the poly(APT-GO) is higher than that of poly(APT) and less than that of GO. Before polymerization of the APT-GO complex, all the NH_2 groups interacted with negatively charged GO, and this interaction facilitated a decreased R_{ct} (small semicircle) value compared to the R_{ct} of GO on the poly(APT-GO) electrode. This indicates that the interaction between APT and GO facilitates a good charge transfer process and helps to reduce the adsorbed oxygen molecules on the electrode surface for the ORR.

Voltammetric characterization of the electrocatalysts for the ORR

The catalytic responses of poly(APT-GO), poly(TCA-GO), and poly(TBA-GO) were examined by employing cyclic voltammetry (CV) and hydrodynamic voltammetry. The GO-containing polymers revealed catalytic properties towards the ORR, as shown in Figure 6(a), as was expected. The ORR current density of the poly(APT-GO) is the highest in a 0.1 M NaOH solution and reveals a 50% higher response compared to poly(TCA-GO) and poly(TBA-GO) at a scan rate of 50 mV/s.

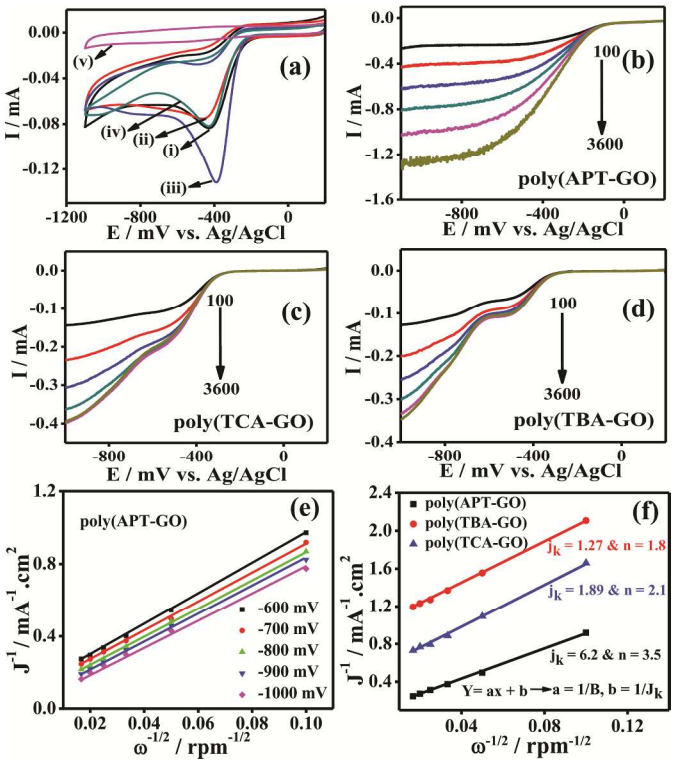

Figure 6. (a) CVs recorded for (i) poly(TBA-GO), (ii) poly(TCA-GO), (iii) poly(APT-GO), and (iv) poly(APT); and in saturated O_2, saturated N_2 for (v) poly(APT-GO) at a scan rate of 50 mV/s. (b) Hydrodynamic voltammograms for (b) poly(APT-GO), (c) poly(TCA-GO), and (d) poly(TBA-GO) with different rotation rates. (e) Koutecky-Levich plots for poly(APT-GO). (f) K-L plots of poly(APT-GO), poly(TCA-GO), and poly(TBA-GO) at –700 mV.

No cathodic peak in the N_2 saturated solution is observed, while in the O_2 saturated solution, there is a significant enhancement of the cathodic peak at –380 mV with a current of 0.133 mA, pointing up the high electrocatalytic activity of the poly(APT-GO). The pure poly(APT) also reveals catalytic activity towards the ORR, but only low acitivity, which might be due to the presence of S and N species in the polymer backbone. In addition, poly(TCA-GO) and poly(TBA-GO) bearing carboxylic acid groups show worse ORR catalytic properties compared with poly(APT-GO), due to the absence of the C–N bond and the amine group in both of the polymer structures. The combination of GO with the polymer supplies sufficient electroactive sites, resulting in more favorable electron transfer kinetics and greatly enhanced electrocatalytic performance towards oxygen reduction on the poly(APT-GO) electrode. The present study shows that the electrocatalytic activity of poly(APT-GO) toward the ORR is significantly enhanced compared with pure GO and pure polymer. We have compared the ORR activity of the monomer-GO complexes (Figure S4 in the SI).). The results indicate very low catalytic activity, and the phenomenon occurs because of the GO-monomer layer are not stable on electrode surface and does not exihibit any conducting properties. Hence, APT-GO, TBA-GO, and TCA-GO complexes show worse ORR activity than poly(APT-GO). Figure 6(b) presents the CVs collected for poly(APT-GO) in oxygen containing 0.1 M NaOH solution as functions of the electrode rotation rate, where the current increases with the increasing rotation rate (from 100 to 3600 rpm). The RDE experiments were also performed on the poly(TCA-GO) (Figure 6(c)) and poly(TBA-GO) (Figure 6(d)) electrodes with the same rotation rate. The limiting current of the ORR for both TCA and TBA composite polymer electrodes containing GO is smaller, and the onset potential for the ORR is more negative than that of poly(APT-GO). The more positive shift of the onset potential with increasing current density on the poly(APT-GO) electrode indicates better catalytic performance than for the other samples, since poly(APT-GO) is rich in nitrogen atoms, while the other two polymers, poly(TBA-GO), and poly(TCA-GO), do not contain nitrogen atoms. Nitrogen atoms play a key role in the ORR process by creating active sites to interact with oxygen molecules. This creation of active sites efficiently facilitates the oxygen reduction pathway, because the resulting C–N bond polarization is expected to weaken the O–O bond, and C–N bonds can be reduced on the electrode surface to form water molecules.[38] The additional significantly high electrochemical performance of poly(APT-GO) can be attributed to its specific structure, containing an electron donating group (e.g., amine) and a C=N– group that is present in monomer structure. After polymerization, there are a large number of imine (C=N–) active sites, thereby increasing the electrocatalytic activity of the poly(APT-GO). The ORR in an aqueous solution is known to occur mainly by two pathways, the direct $4e^-$ transfer pathway and/or a $2e^-$ transfer pathway, where the direct $4e^-$ pathway is related to H_2O formation from adsorbed molecular oxygen without the formation of peroxide intermediates.[39] In the fuel cell, the direct $4e^-$ pathway is

absolutely preferred. The ORR activities and kinetic parameters were evaluated using the Koutecky-Levich (K-L) equations [Eqs. (1) and (2)]:

$$\frac{1}{J} = \frac{1}{J_L} + \frac{1}{J_K} = \frac{1}{B\omega^{1/2}} + \frac{1}{J_K} \quad (1)$$

$$B = 0.62nFC_0(D_0)^{2/3}\upsilon^{-1/6} \quad (2)$$

Where J denotes the measured current density, J_K and J_L are the kinetic and diffusion-limited current densities, ω is the angular velocity of the disk ($\omega = 2\pi N$, where N denotes the linear rotation rate), n denotes the overall number of electrons transferred, F is the Faraday constant (96485 C mol^{-1}), C_O denotes the bulk concentration of O_2 (1.26×10^{-3} mol L^{-1}), D_O is the diffusion coefficient of O_2 (1.93×10^{-5} cm^2 s^{-1}), and υ is the kinetic viscosity of the electrolyte (1.0×10^{-2} cm^2 s^{-1}). Thus, to determine the kinetic proficiencies of poly(APT-GO), the well-known K-L plots were obtained for the ORR at various rotation speeds. The K-L plots at the different electrode potentials (Figure 6(e)) show good linearity and approximately constant slopes within the given potential range (–600 to –1100 mV), which suggests that the linearity and parallelism of the plots are characteristic of first order reaction kinetics. Figure S5(a) and S5(b) in the SI presents the K-L plots obtained for the poly(TCA-GO) and poly(TBA-GO) electrodes at different potentials (–600 to –1100 mV). As shown in Figure 6(f), the n values and J_k values can be determined from the intercepts of the K-L plots, respectively, by using Equation (2).

We compared the catalytic activity of poly(APT-GO) with poly(APT), and poly(APT-RGO) (where reduced graphene oxide (RGO) was compared, because it has higher conductivity than GO), and with commercially available Pt/C electrodes employing hydrodynamic voltammwtry at a rotation rate of 1600 rpm (Figure 7 (a)). The inset of this figure shows that the onset potential of poly(APT-GO) is approximately –30 mV, revealing the efficient catalytic reduction of oxygen. The E_{onset} is positively shifted compared to poly(APT-RGO) (–62 mV) and poly(APT) (–100 mV), and the ORR current density is also higher at the poly(APT-GO) electrode compared to the poly(APT-RGO) and poly(APT) electrodes. The electrocatalytic activity of poly(APT-GO) is best in terms of limiting current density, but the E_{onset} remains slightly lower than that of the Pt/C electrode. Thus, the present preparation method can be used to simply convert APT monomer and GO into a non-metal ORR electrocatalyst by a simple and scalable electropolymerization technique, suggesting a significant reason to investigate the cost-effective preparation of various nonmetal catalytic materials for fuel cells. Electron transfer numbers on the modified electrodes were found to be dependent on the potential (–600 to –1100 mV) within the range of $n \geq 3.5$. This suggests that poly(APT-GO) causes the ORR to proceed by the four-electron ($4e^-$) pathway, which is a desirable ORR pathway. Figure 7(b) shows that the $4e^-$ ORR reaction commences at approximately –700 mV for poly(APT-GO) and –1200 mV for poly(APT-RGO) electrodes, while the pure poly(APT) shows the catalytic property towards a two-electron ($2e^-$) transfer process at all potentials. This result suggests that poly(APT-GO) is a much more efficient ORR electrocatalyst than pure poly(APT) and poly(APT-RGO), consistent with the relatively high calculated kinetic current density J_K for the ORR at the poly(APT-GO) electrode compared to the poly(APT) and poly(APT-RGO) electrodes (Figure S6(a) in the SI). Inset from the Figure 7 (b) explains the Tafel slope of the poly(APT-GO) and Pt/C electrodes. The slopes obtained at kinetic region between –0.1 to –0.3 V and the values were 97.0 and 58.0 mV/dec. for poly(APT-GO) and Pt/C catalyst, respectivelly. The smaller Tafel slope indicates faster electron transfer kinetics. However, the poly(APT-GO) Tafel slope is demonstrating reasonable behaviour to that of commercial Pt/C catalyst. To evaluate the practical properties of the proposed electrocatalyst, the crossover effects and stability of the catalyst were examined. When Pt is used as an electrocatalyst on both anode and cathode electrodes in direct methanol fuel cells (DMFCs), the Pt has tendency to be oxidized on the surface, causing the loss of cell voltage by "methanol or ethanol crossover", in which appreciable amounts of methanol or ethanol leak into the cathode chamber. Thus, the electrocatalytic performances of poly(APT-GO) and commercial Pt/C catalysts were measured against the electrooxidation of methanol and ethanol as shown in Figure 7(c). When 2.0 M methanol or ethanol was added to the solution, the ORR current at the poly(APT-GO) electode did not exhibit any obvious change, while the Pt/C catalyst suffered a sharp decrease and even changed to a negative current as a result of the mixed potential. The durability of the poly(APT-GO) and Pt/C catalysts was also compared. The catalysts were exposed to –300 mV for 45,000 s in an O_2 saturated 0.1 M NaOH solution.

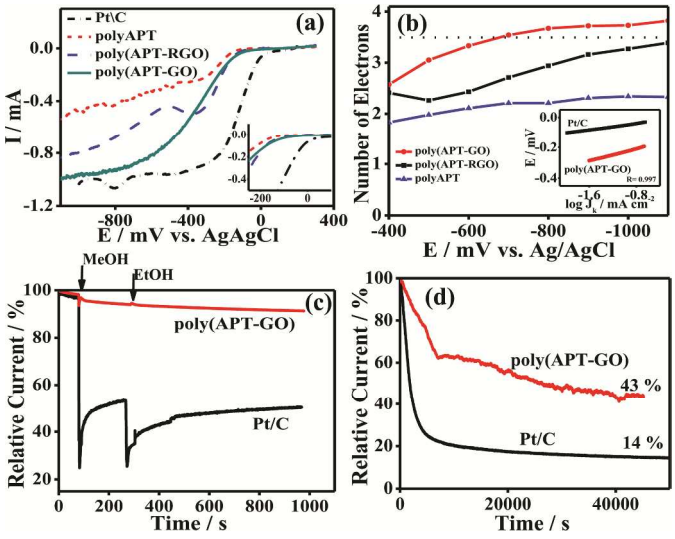

Figure 7. (a) Hydrodynamic voltammograms for poly(APT), poly(APT-GO), poly(APT-RGO), and 60% Pt/C electrodes at 1600 rpm (inset is an enlargement of the onset potential region). (b) Potential dependence of the electron transfer

number for the poly(APT), poly(APT-GO), and poly(APT-RGO) electrodes (inset from this figure explains the Tafel plot of poly(APT-GO) and Pt/C electrodes). (c) Chronoamperometry curves (i *vs*.t) for the ORR at the poly(APT-GO) and 60% Pt/C electrodes. MeOH and EtOH (2 M) were added at different intervals. (d) Long-term stability towards the ORR at the poly(APT-GO) and 60% Pt/C in O_2 saturated 0.1 M NaOH solution at –300 mV.

As shown in Figure 7(d), the chronoamperometric response for poly(APT-GO) in 0.1 M NaOH solution exhibited very slow attenuation, and 43% of the current persisted after 45,000 s. In contrast, the Pt/C electrode exhibited a gradual decrease, where approximately 14% of initial current remained after the same period, which is likely caused by the aggregation of Pt nanoparticles. We also performed continuous potential cycling between +100 and –1200 mV to investigate the stability of the poly(APT-GO) electrode towards the ORR in 0.1 M NaOH. As is shown in Figure S6(b) in the SI, no obvious decrease in the current was observed after 15,000 continuous cycles. These measurements confirm that the poly(APT-GO) catalyst demonstrates better stability and resistance towards methanol and ethanol crossover, which overcomes a main challenge faced by metal-based catalysts in FCs. As a result, poly(APT-GO) is much more stable than the commercially available Pt/C, with potential uses in direct methanol and alkaline fuel cells.

Conclusions

We have successfully developed a facile electrochemical approach for the synthesis of functionalized polyterthiophenes anchored GO from organic monomer-GO complexes as electrocatalysts. The monomer complexes and their polymers anchored GO were evaluated by employing FTIR, XPS, FE-SEM, and HR-TEM measurements. The TGA results show the high thermal stability of the monomer-GO complexes, and the effective electrochemical catalytic properties were evaluated using impedance spectroscopy, cyclic voltammetry, and RDE experiments. The poly(APT-GO) electrode exhibited the highest catalytic activity towards O_2 reduction and afforded facile 4e- transfer for the ORR, whereas the carboxyl group-bearing polymer-GO electrodes showed only $2e^-$ transfer. The long-term stability and tolerance to the crossover of alcohol are also better than that of Pt/C. The amine-containing polyterthiophenes incorporating GO retained a large number of imine (C=N–) active sites, was also affected by the C–N bond and featured enhanced ORR performance. This simple methodology gives notable technical advantages, including easy tuning of the electronic properties of terthiophene conducting polymers with carbon materials. Furthermore, the amine-containing polyterthiophenes can be used in applications that require more efficient electrochemical catalysts that are metal-free.

Acknowledgement

This work was supported through a National Research Foundation grant funded by the Ministry of Education, Science and Technology (MEST) of the Republic of Korea (grant no. 20100029128).

Notes and references

[a] Department of Chemistry, Pusan National University, Busan 609-735, Republic of Korea.
[b] Institute for Superconducting and Electronic Materials, Australian Institute for Innovative Materials, University of Wollongong, North Wollongong, NSW 2500, Australia.
[*] E-mail: ybshim@pusan.ac.kr, jhk@uow.edu.au

† Electronic Supplementary Information (ESI) available: Structures of all the monomers, HR-TEM images of GO, XPS data, additional K-L plots, and stability results. See DOI: 10.1039/b000000x/

(1) R. P. O'Hayre, S. W. Cha, W. G. Colella and F. B. Prinz, *Fuel Cell Fundamentals*, John Wiley & Sons, New York, 2006.
(2) F. Barbir, *PEM Fuel Cells Theory and Practice,* 2nd ed., Academic Press: 225 Wyman Street, Waltham, USA, 2012.
(3) B. C. H. Steele and A. Heinzel, *Nature,* 2001, **414**, 345.
(4) K. Gong, F. Du, Z. Xia, M. Durstock and L. Dai, *Science,* 2009, **323**, 760.
(5) J. O'M. Bockris and S. U. M. Khan, *Surface Electrochemistry*; Plenum Press: New York, 1993.
(6) Y. Zhang, T. Han, J. Fang, P. Xu, X. Li, J. Xu and C-C. Liu, *J. Mater.Chem. A*, 2014, **2**, 11400.
(7) M. K. Dede, *Nature,* 2012, **486**, 43.
(8) Z. Zhang, C. Zhang, J. Sun, T. Kou, Q. Bai, Y. Wang and Y. Ding, *J. Mater. Chem. A*, 2013, **1**, 3620.
(9) R. Bashyam and P. Zelenay, *Nature,* 2006, **443**, 63.
(10) G. Inzelt, *Conducting polymer: A New Era in Electrochemistry*; Springer-Verlag: Berlin, 2012.
(11) D. T. McQuade, A. E. Pullen and T. M. Swager, *Chem. Rev.,* 2000, **100**, 2537.
(12) H. B. Noh, M.S. Won, N. H. Kwon, S. Shin and Y. B. Shim, *Biosens. Bioelectron.*, 2010, **25**, 1735.
(13) T. Y. Lee and Y. B. Shim, *Anal. Chem*., 2001, **73**, 5629.
(14) D. H. Kim, J. H. Kim, T. H. Kim, D. M. Kang, Y. H. Kim, Y. B. Shim and S. C. Shin, *Chem. Mater*., 2003, **15**. 825
(15) X. Wang, K. Maeda, A. Thomas, K. Takanabe, G. Xin, J. M. Carlsson, K. Domen and M. Antoniett, *Nat. Mater*., 2009, **8**, 76.
(16) B. Winther-Jensen, O. Winther-Jensen, M. Forsyth and D. R. MacFarlane, *Science,* 2008, **321**, 671.
(17) D. Wang, S. Lu, P. J. Kulesza, C. M. Li, R. D. Marco and S. P. Jiang, *Phys.Chem.Chem.Phys*., 2011, **13**, 4400.
(18) R. P. Kingsborough and T. M. Swager, *Chem. Mater.,* 2000, **12**, 872.
(19) M. Boopathi, M. S. Won, Y. H. Kim, S. C. Shin and Y. B. Shim, *J. Electrochem. Soc*., 2002, **149**, E265.
(20) W. M. Millán, T. T. Thompson, L. G. Arriaga and M. A Smit, *Int. J. Hydrogen Energy,* 2009, **34**, 694.
(21) V. G. Khomenko, V. Z. Barsukov and A. S. Katashinskii, *Electrochim. Acta*, 2005, **50**, 1675.
(22) N. Oyama, N. Oki, H. Ohno, Y. Ohnuki, H. Matsuda and E. Tsuchida, *J. Phys. Chem.*, 1983, **87**, 3642.

(23)H. Park, T. G. Kwon, D. S. Park and Y. B. Shim, *Bull. Korean Chem. Soc.*, 2006, **27**, 1763.
(24)H. Liu, G. Zhang, Y. Zhou, M. Gao and F. Yang, *J. Mater. Chem. A*, 2013, **1**, 13902.
(25)J. Liang, Y. Jiao, M. Jaroniec and S. Z. Qiao, Angew. Chem., Int. Ed., 2012, **51**, 11496.
(26)A. Ambrosi, C. K. Chua, A. Bonanni and M. Pumera, *Chem. Rev.*, 2014, **114**, 7150.
(27)L. R. Gong, (Ed.), *New Progress on Graphene Research*; InTech Publishing Co.: 2013.
(28)D. C. Marcano, D. V. Kosynkin, J. M. Berlin, A. Sinitskii, Z. Sun, A. Slesarev, L. B. Alemany, W. Lu and J. M. Tour, *ACS Nano,* 2010, **4**, 4806.
(29)D. R. Dreyer, S. Park, C. W. Bielawski and R. S. Ruoff, *Chem. Soc. Rev.,* 2010, **39**, 228.
(30)Z. Yang, Z. Yao, G. Li, G. Fang, H. Nie, Z. Liu, X. Zhou, X. A. Chen and S. Huang, *ACS Nano*, 2012, **6**, 205.
(31)Y. H. Kim, J. Hwang, J. I. Son and Y. B. Shim, *Synth. Met.,* 2010, **160**, 413.
(32)D. M. Kim, K. B. Shim, J. I. Son, S. S. Reddy and Y. B. Shim, *Electrochim. Acta,* 2013, **104**, 322.
(33)Q. Wu, Y. Sun, Y. Bai and G. Shi, *Phys. Chem. Chem. Phys.,* 2011, **13**, 11193.
(34)S. Park, D. A. Dikin, S. T. Nguyen and R. S. Ruoff, *J. Phys. Chem. C,* 2009, **113**, 15801.
(35)H. Yang. C. Shan, F. Li, D. Han, Q. Zhang and L. Niu, *Chem. Commun.,* 2009, **26**, 3880.
(36)B. R. Stepp and S. T. Nguyen, *Macromolecules,* 2004, **37***,* 8222.
(37)S. Park, J. An, R. D. Pinar, I. Jung, D. Yang, A. Velamakanni, S. T. Nguyen and R. S. Ruoff, *Chem. Mater*., 2008, **20**, 6592.
(38)G. Tuci, C. Zafferoni, P. D'Ambrosio, S. Caporali, M. Ceppatelli, A. Rossin, T. Tsoufis, M. Innocenti and G. Giambastiani, *ACS Catal*., 2013, **3**, 2108.
(39) E. Yeager, *J. Electrochem. Soc*., 1981, **128**, 160C.

Table of Contents

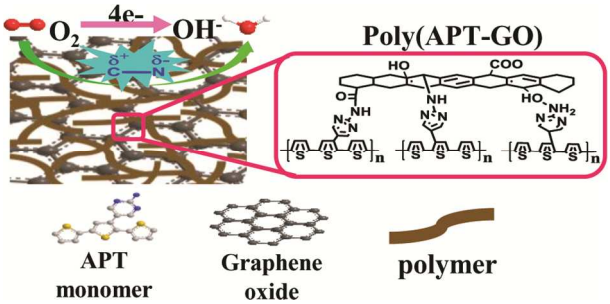

A new polyterthiophene anchored GO based ORR electrocatalyst was prepared, C–N bond containing aminopyrimidyl groups on polymer structure serve as active sites with better and stable activity of ORR.